A Joint ND280-SK 1R$_\mu$-SK 1R$_e$ Fit using MCMC

Asher Kaboth[1], Richard Calland[2], and Dave Payne[2]

[1]Imperial College London

[2]University of Liverpool

February 17, 2014

Abstract

An analysis of the Run 1–4 T2K data is performed with a Markov Chain Monte Carlo. The data included in the analysis are the ND280 ν_μ, SK 1R$_\mu$, and SK 1R$_e$ samples. When fitting with only T2K data, the best fit point for the oscillation parameter is $\Delta m^2_{32} = 2.491 \times 10^{-3}$ eV^2, $\sin^2\theta_{23} = 0.520$, and $\sin^2\theta_{13} = 0.0377$ for normal hierarchy and $\delta_{cp} = 0$, with 90% credible intervals of 2.34–2.69$\times 10^{-3}$ eV^2, 0.445–0.595, and 0.0230–0.0600, respectively. When fitting with the reactor constraint, the best fit point for normal hierarchy is $\Delta m^2_{32} = 2.510 \times 10^{-3}$ eV^2, $\sin^2\theta_{23} = 0.527$, and $\delta_{cp} = -1.551$. The 90% credible interval for δ_{cp} excludes 0.45–2.66 for the normal hierarchy and 0.15–3.04 for inverted hierarchy. Other interpretations of the data are also discussed.

T2K-TN-171

Contents

1 Introduction

This technical note describes a fit to the ND280 tracker ν_μ, SK 1R$_\mu$, and SK 1R$_e$ Run 1–4 data using the Markov Chain Monte Carlo method. A description of the Markov Chain method can be found in [1].

This analysis uses two new features compared to the method described the referenced note; instead of reweighting the predicted Monte Carlo (MC) spectra using binned pdf templates, the individual MC events are weighted event-by-event, according to the relevant variable(s) for the tweak being applied. Then, when all weights have been calculated, the MC events are binned to create the predicted spectra.

Additionally, the method to find the best fit point has been changed, due to the increased number of interesting oscillation variables. The fitter now uses an adaptive kernel density method to smooth the posterior and find the maximal point. This method is described in Section 5.

The Bayesian probability function used to fit the data depends on the data sample and flux, cross section, detector, and final state interactions (FSI) systematics, which will be described in subsequent sections. This function has the form:

$$
\begin{aligned}
-\ln(P) = &\sum_{i}^{ND280bins} N_i^p(\vec{b},\vec{x},\vec{f},\vec{d}) - N_i^d + N_i^d ln[N_i^d/N_i^p(\vec{b},\vec{x},\vec{f},\vec{d})] \\
&+ \sum_{i}^{SK1R_\mu bins} N_i^p(\vec{b},\vec{x},s\vec{k}d) - N_i^d + N_i^d ln[N_i^d/N_i^p(\vec{b},\vec{x},s\vec{k}d)] \\
&+ \sum_{i}^{SK1R_e bins} N_i^p(\vec{b},\vec{x},s\vec{k}d) - N_i^d + N_i^d ln[N_i^d/N_i^p(\vec{b},\vec{x},s\vec{k}d)] \\
&+ \frac{1}{2}\sum_{i}^{E_\nu bins}\sum_{j}^{E_\nu bins} \Delta b_i (V_b^{-1})_{i,j} \Delta b_j \\
&+ \frac{1}{2}\sum_{i}^{xsecpars}\sum_{j}^{xsecpars} \Delta x_i (V_x^{-1})_{i,j} \Delta x_j \\
&+ \frac{1}{2}\sum_{i}^{fsipars}\sum_{j}^{fsipars} \Delta f_i (V_f^{-1})_{i,j} \Delta f_j \\
&+ \frac{1}{2}\sum_{i}^{nd280det}\sum_{j}^{nd280det} \Delta d_i (V_d^{-1})_{i,j} \Delta d_j \\
&+ \frac{1}{2}\sum_{i}^{skdet}\sum_{j}^{skdet} \Delta skd_i (V_{skd}^{-1})_{i,j} \Delta skd_j
\end{aligned}
\tag{1}
$$

where V_{ij} represents covariance matrices constraining systematic parameters labeled by b for flux, x for cross section, f for FSI, d for ND280 detector, and skd for SK detector. N_i^p is the number of predicted events in a particular bin, given the values of the systematic parameters, and N_i^d is the number of data events.

2 Event Selection

2.1 ND280 Tracker ν_μ

The 2013 tracker ν_μ selection is described in T2K-TN-152 [2]. The charged-current inclusive (CCInc) is divided into three subsamples: charged-current 0-π (CC0π), charged-current single π^+ (CC1π), and charged-current other (CCoth). The sample is subdivided in order to isolate topologies of interest for constraining cross section systematics.

The inclusive sample is defined by the following cuts:

1. Good Data Quality: the global ND280 data quality flag must be good

2. Bunching: Tracks considered part of the same event must be in the same beam bunch

3. TPC Quality and Fiducial Volume: There must be at least one track beginning in FGD1's fiducial volume, and entering a TPC with at least 18 vertical TPC clusters

4. Backwards-going and TPC1 veto: if there is activity in TPC1, or if the end position of the highest momentum track is more upstream than the start position, the track is vetoed

5. Broken Tracks FGD1: Events are rejected when the muon candidate's z start position is more than 425 mm away from the FGD1 upstream edge and in the same event where at least one "FGD-only" track with its start position out the FGD1 fiducial volume exists.

6. Muon PID: The highest momentum negative track in the event must be muon-like, according to TPC PID

The CC0π sample is further defined by rejecting events with any pion reconstructed in the TPC, any electrons or positrons in the TPC, or any Michel electrons or pions reconstructed in the FGDs.

The CC1π sample is further defined by rejecting events with negative pions or electrons or positrons in the TPC and selecting events where there is one reconstructed positive pion or one Michel electron reconstructed in the TPCs and FGDs.

The CCoth sample contains all other CCInc events not in the CC0π or CC1π samples.

The binning for the samples chosen for fitting is finer than the binning from the 2012 analysis, and is chosen to be as fine as possible while still requiring at least 25 MC events in each bin. The binning procedure is described in [2]. The bins are:

- CC0π and CCoth
  - p_μ (MeV): 0, 300, 400, 500, 600, 700, 800, 900, 1000, 1250, 1500, 2000, 3000, 5000, 30000
  - $\cos\theta$: -1.0, 0.6, 0.7, 0.8, 0.85, 0.9, 0.92, 0.94, 0.96, 0.98, 0.99, 1.0
- CC1π

- p_μ (MeV): 0, 300, 400, 500, 600, 700, 800, 900, 1000, 1250, 1500, 2000, 5000, 30000
- $\cos\theta$: -1.0, 0.6, 0.7, 0.8, 0.85, 0.9, 0.92, 0.94, 0.96, 0.98, 0.99, 1.0

The data samples are shown in Figure 1. Table 1 gives the number of events in the 0–30 GeV muon momentum region for the three samples and the CC inclusive total sample.

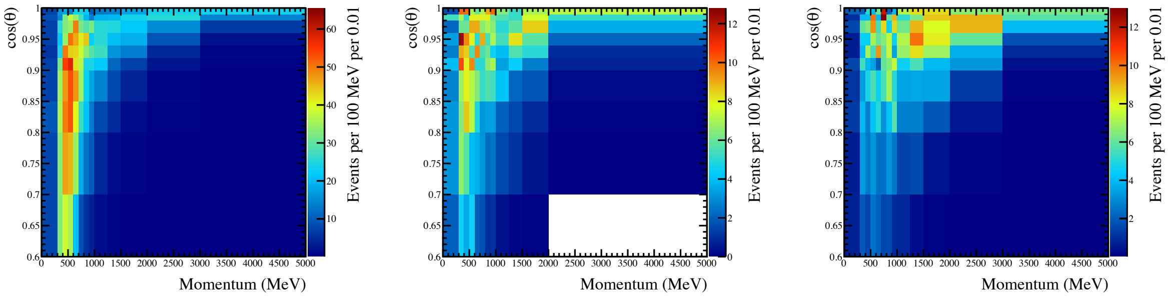

Figure 1: The data samples for this analysis. Shown in (a) is the CC0π sample, in (b) the CC1π sample, and in (c) the CCoth sample.

Table 1: Number of data events in the three subsamples and the inclusive sample.

CC0π	CC1π	CCoth	CCInc
17369	4047	4173	25589

2.2 SK 1R$_e$ and 1R$_\mu$

The selection for the SK data samples in 2013 is described in TN-148 [3]. For the 1R$_e$ events, the selection is as follows:

1. Fully-contained fiducial volume
2. One ring found by the ring counting algorithm
3. The ring is identified as electron-like by the PID algorithm
4. Visible energy (E_{vis}) is greater than 100 MeV

5. Zero decay electrons
6. Reconstructed neutrino energy (E_{rec}) is less than 1250 MeV
7. fiTQun π^0 cut of $\ln(L_{\pi^0}/L_e) < 175 - 0.875 \times m_{\pi^0}$

There are 28 total events in this sample.

For the 1R$_\mu$ events, the selection is as follows:

1. Fully-contained fiducial volume event
2. One ring found by the ring counting algorithm
3. The ring is identified by the PID as muon-like
4. Reconstructed momentum is greater than 200 MeV/c
5. Number of decay electrons is equal or less than one

There are 120 total events in this sample.

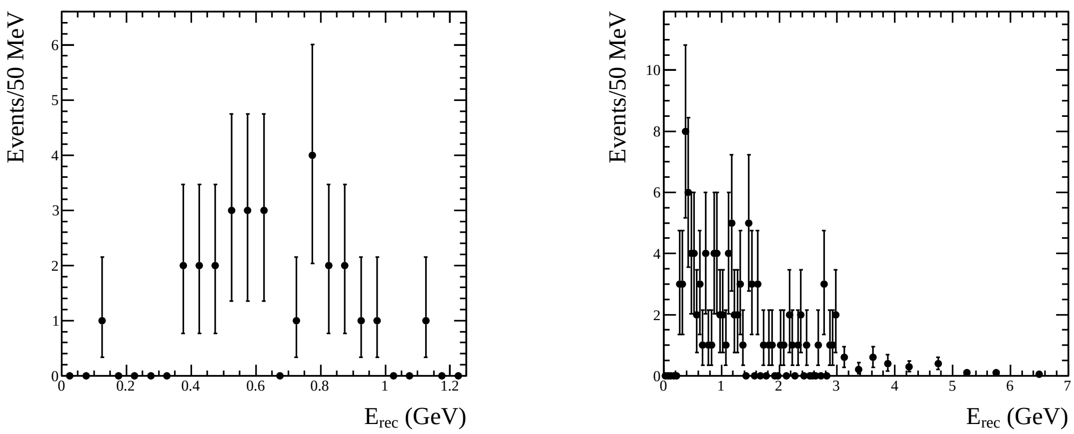

Figure 2: SK data samples for Runs 1–4. Left plot shows 1R$_e$ and right plot 1R$_\mu$. The fit window for the 1R$_\mu$ events extends to 30 GeV, but no events are found above 7 GeV, so the data is only shown up to this limit for clarity.

3 Systematic Errors

3.1 Flux

The flux systematic errors are from TN-099 [4]. The covariance matrix is binned in 11 bins for ν_μ, 5 bins for $\bar{\nu}_\mu$, 7 bins for ν_e, and 2 bins for $\bar{\nu}_e$ for both ND280 and SK as follows, in true neutrino energy (GeV):

- ν_μ: 0.0, 0.4, 0.5, 0.6, 0.7, 1.0, 1.5, 2.5, 3.5, 5.0, 7.0, 30.0
- $\bar{\nu}_\mu$: 0.0, 0.7, 1.0, 1.5, 2.5, 30.0
- ν_e: 0.0, 0.5, 0.7, 0.8, 1.5, 2.5, 4.0, 30.0
- $\bar{\nu}_e$: 0.0, 2.5, 30.0

Figure 3 shows the flux covariance matrix.

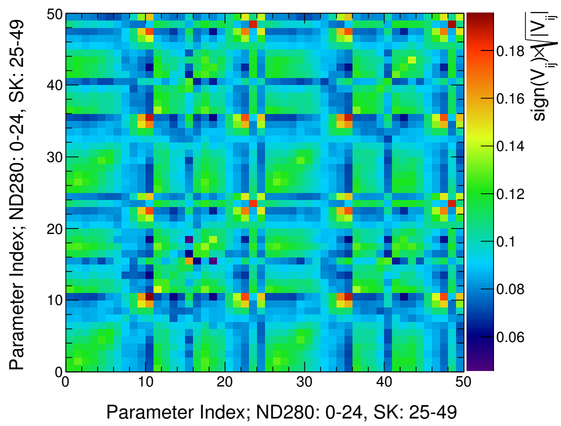

Figure 3: The flux covariance matrix used in the analysis. The bin indices are as follows: ND280 ν_μ (0-10), ND280 $\bar{\nu}_\mu$ (11-15), ND280 ν_e (16-22), ND280 $\bar{\nu}_e$ (23-24), SK ν_μ (25-35), SK $\bar{\nu}_\mu$ (36-40), SK ν_e (41-47), and SK $\bar{\nu}_e$ (48-49), with the energy divisions for the neutrino types given in the text.

Flux weights are applied on an event-by-event basis to the MC events depending on the true neutrino energy of the event.

3.2 Cross Section

The cross section parameterization is largely unchanged from the 2012 analysis. The relevant parameters are given in Table 2. All parameters are independent from one another, excepting M_A^{RES}, CC1π E1, and NC1π^0, which have correlations between them as detailed in [5].

The two types of systematic, shape and normalization, are treated differently. For the shape parameters, the treatment is different between ND280 and SK. At ND280 a spline is created using T2KReWeight for each MC event. This spline is then evaluated for the desired reweighting value of the parameter, and that weight is applied to the event. At SK, splines are created in binned E_{rec} and E_{true}. Each MC event is weighted according to the evaluated spline for the kinematic bin of that event. For the normalization parameters, the event is simply weighted by the value of the parameter.

3.3 ND280 Detector

The detector systematics for this analysis are described in the tracker selection technical note [2]. For an MCMC analysis, the method of reanalyzing every event for every step was computationally prohibitive, taking approximately 3s to reweight each step. Therefore, a covariance matrix approach was used, similar to the 2012 method. The covariance matrix was produced by 2000 throws of the inputs for the detector systematics, and the full detector systematic analysis was used for each throw. The covariance for each bin of the matrix was calculated as

$$V_{ij} = \frac{1}{2000} \sum_{n=1}^{2000} \frac{\left(N_n^{\text{reweighted},i} - N^{\text{average},i}\right)\left(N_n^{\text{reweighted},j} - N^{\text{average},j}\right)}{N^{\text{average},j} N^{\text{average},i}} \tag{2}$$

where $N^{\text{average},i}$ is the average of the 2000 throws.

The binning for the detector systematic covariance matrix was chosen to be coarser than the binning used for fitting the data, in order to reduce the number of parameters used in the fit, especially as the size of the detector systematic errors is typically smaller than the size of the flux and cross section errors. The binning chosen for all samples has seven bins in momentum and five bins in $\cos\theta$ and is as follows:

Table 2: NIWG 2012a cross section parameters for the fit, showing the applicable range of neutrino energy, nominal value and prior error. The type of systematic (shape or normalization) is also shown.

Parameter	E_ν Range	Nominal	Error	Class
M_A^{QE}	all	1.21 GeV/c^2	0.45	shape
M_A^{RES}	all	1.41 GeV/c^2	0.11	shape
p_F ^{12}C	all	217 MeV/c	30	shape
E_B ^{12}C	all	25 MeV	9	shape
SF ^{12}C	all	0 (off)	1 (on)	shape
CC Oth shape ND280	all	0.0	0.40	shape
p_F ^{16}O	all	225 MeV/c	30	shape
E_B ^{16}O	all	27 MeV	9	shape
SF ^{16}O	all	0 (off)	1 (on)	shape
CC Oth shape SK	all	0.0	0.40	shape
W-Shape	all	0.0	0.20	shape
Pionless Delta Decay	all	0.0	0.2	shape
CCQE E1	$0 < E_\nu < 1.5$	1.0	0.11	norm
CCQE E2	$1.5 < E_\nu < 3.5$	1.0	0.30	norm
CCQE E3	$E_\nu > 3.5$	1.0	0.30	norm
CC1π E1	$0 < E_\nu < 2.5$	1.15	0.43	norm
CC1π E2	$E_\nu > 2.5$	1.0	0.40	norm
CC Coh	all	1.0	1.0	norm
NC1π^0	all	0.96	0.43	norm
NC 1$\pi^\pm$	all	1.0	0.3	norm
NC Coh	all	1.0	0.3	norm
NC other	all	1.0	0.30	norm
ν_μ/ν_e	all	1.0	0.03	norm
$\nu/\bar{\nu}$	all	1.0	0.40	norm

- p_μ (MeV): 0, 300, 500, 600, 700, 1000, 2000, 30000
- $\cos\theta$: -1, 0.85, 0.9, 0.94, 0.98, 1.0

The covariance matrix is shown in Figure 4. In this matrix, bins 0-34 cover the CC0π sample, 35-69 the CC1π sample, and 70-104 the CCoth sample. Within each sample, the bins iterate over $\cos\theta$ from low to high for the lowest momentum bin, then from low to high for the second lowest momentum bin, etc.

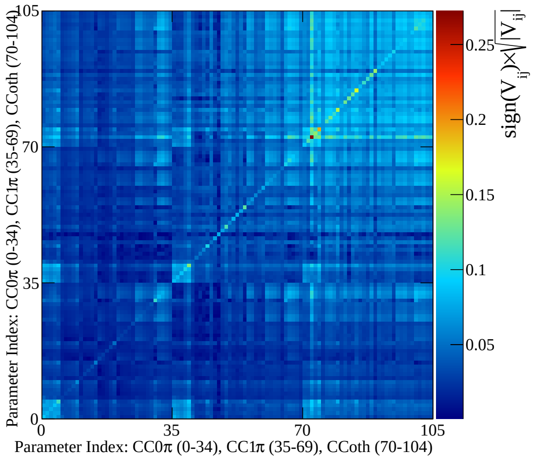

Figure 4: The detector covariance matrix used in the analysis. In this matrix, bins 0-34 cover the CC0π sample, 35-69 the CC1π sample, and 70-104 the CCoth sample. Within each sample, the bins iterate over $\cos\theta$ from low to high for the lowest momentum bin, then from low to high for the second lowest momentum bin, etc.

To apply this systematic, each event is weighted by the value according to the bin corresponding to the event's reconstructed momentum and angle.

3.4 Final State Interactions (ND280 only)

In previous ND280 analyses, the final state interaction systematics were combined with the detector systematics. However, due to the new treatment of the detector systematics, the FSI is no longer included. For this analysis, the six FSI parameters described in [5] (Pion production, 'PION_PROD'; pion absorption 'PION_ABS'; low and high energy charge exchange, 'CEX_LO' and 'CEX_HI'; and low and high energy inelastic interactions, 'INEL_LO' and 'INEL_HI') are treated as independent. That is

$$
\begin{aligned}
&W_{FSI}(\sigma_{INEL\_LO}, \sigma_{INEL\_HI}, \sigma_{PION\_PROD}, \sigma_{PION\_ABS}, \sigma_{CEX\_LO}, \sigma_{CEX\_HI}) = \\
&W(\sigma_{INEL\_LO}) \times W(\sigma_{INEL\_HI}) \times W(\sigma_{PION\_PROD}) \times \\
&W(\sigma_{PION\_ABS}) \times W(\sigma_{CEX\_LO}) \times W(\sigma_{CEX\_HI})
\end{aligned}
$$

A covariance matrix was created from the variations in Table 1 of [5], and is shown in Figure5.

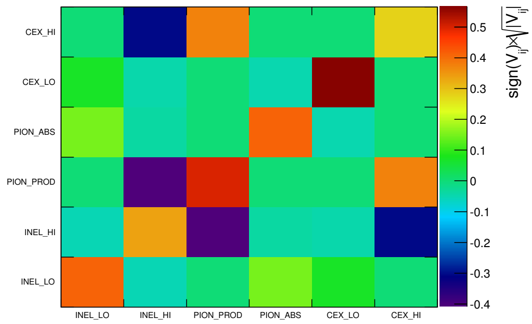

Figure 5: The FSI covariance matrix used in the analysis. The parameters are defined in the NIWG 2012a technical note. [5]

For each parameter, a spline is created using T2KReWeight for each MC event. This spline is then evaluated for the desired reweighting value of the parameter, and that weight is applied to the event.

3.5 SK Detector

The SK detector systematics are correlated between the 1R$_e$ and 1R$_\mu$ samples, as described in TN-186 [6]. The first 12 parameters are for the 1R$_e$ sample, in four sets of three energy bins (0–0.35; 0.35–0.8; 0.8–1.25 GeV) for the signal ν_e, beam ν_μ CC, beam ν_e CC, and NC events. The next 6 parameters are for 1R$_\mu$: three energy bins (0–0.4; 0.4-1.1; 1.1-30 GeV) for ν_μ CCQE, one bin for ν_μ CCnQE, one bin for ν_e CC, and one bin for NC events. The final bin is the energy scale error.

The covariance matrix is shown in Figure 6. The matrix contains the FSI+SI errors for SK.

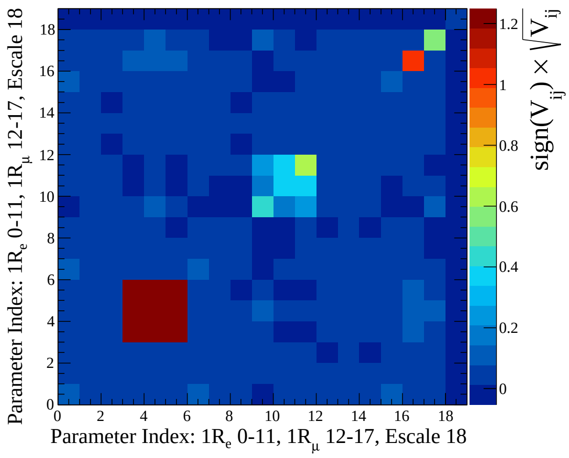

Figure 6: The SK detector covariance matrix used in the analysis. The errors for 1R$_e$ are in bins 0-11, 1R$_\mu$ in bins 12-17, and the energy scale error in bin 18.

4 Monte Carlo Predictions and Pre-fit Data/MC comparison

4.1 ND280

This analysis uses Production 5E/F MC to generate the predicted spectra for the samples. The raw MC undergoes two tunings to generate the initial predicted distributions. First, the events are tuned according to the 11bv3.2 tuning including Run 4 data. Secondly, the events are tuned for the non-nominal values of the cross section parameters M_A^{RES}, CC1π E1, and NC1π0 according to a fit to the MiniBoone CC1π data as described in [5]. Table 3 gives the number of events in the 0–30 GeV/c muon momentum region for the data and the MC.

The nominal MC prediction for the is shown in Figure 7. The ratio of data to nominal MC is shown in Figure 8. Projections of the data and nominal MC in momentum and angle are shown in Figures 9 and 10. Generally, the MC predicts

Table 3: Number of data events in the three subsamples and the inclusive sample.

	CC0π	CC1π	CCoth	CCInc
Data	17369	4047	4173	25589
MC	19978.2	4953.2	4544.26	29475.6
Data/MC Ratio	0.869	0.817	0.918	0.868

a larger number of events than the data, with the effect more pronounced in the CC0π and CC1π samples than in the CCoth sample.

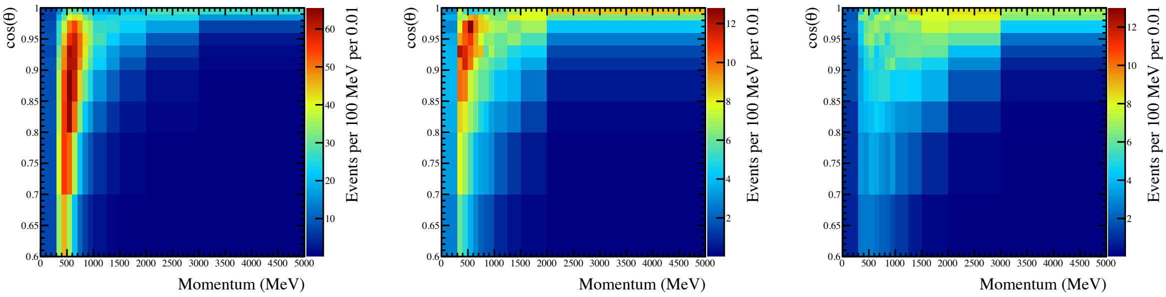

Figure 7: The nominal number of MC predicted events in the p–$\cos\theta$ binning used for the fit. The highest momentum and backwards angle bins are not shown for clarity. Shown in (a) is the CC0π sample, in (b) the CC1π sample, and in (c) the CCoth sample.

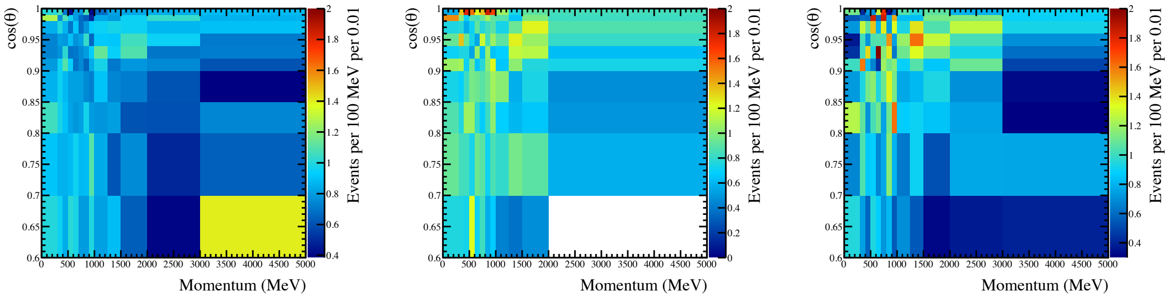

Figure 8: The ratio between the data events and the nominal number of MC events in the p–$\cos\theta$ binning used for the fit. Shown in (a) is the CC0π sample, in (b) the CC1π sample, and in (c) the CCoth sample.

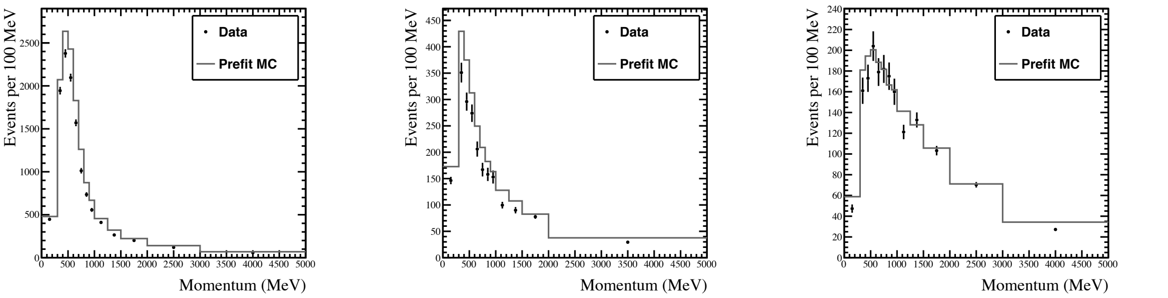

Figure 9: The data and predicted number of MC events projected onto the momentum axis. Shown in (a) is the CC0π sample, in (b) the CC1π sample, and in (c) the CCoth sample.

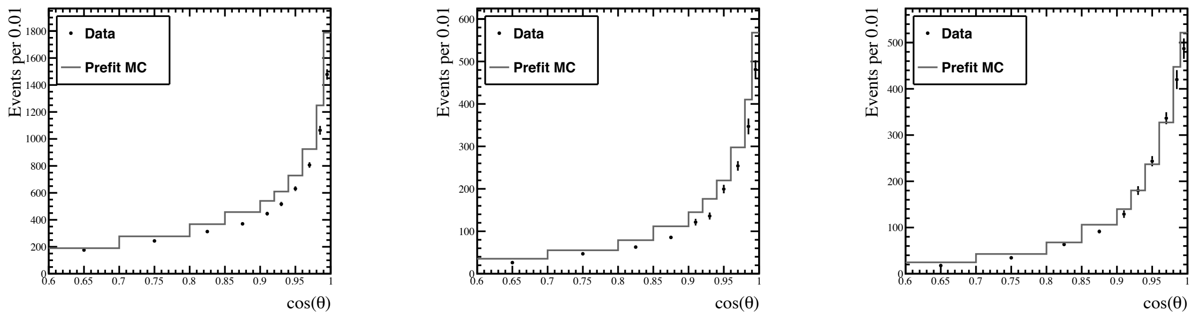

Figure 10: The data and predicted number of MC events projected onto the $\cos\theta$ axis. Shown in (a) is the CC0π sample, in (b) the CC1π sample, and in (c) the CCoth sample.

4.2 SK 1R$_\mu$

This analysis uses SKMC v13a to generate the predicted spectra for the samples. The raw MC undergoes two tunings to generate the initial predicted distributions. First, the events are tuned according to the 11bv3.2 tuning including Run 4 data. Secondly, the events are tuned for the non-nominal values of the cross section parameters M_A^{RES}, CC1π E1, and NC1π0 according to a fit to the MiniBoone CC1π data as described in [5]. Table 4 gives the number of events in the 0–30 GeV reconstructed energy range, broken down by sample type and interaction mode. Additionally, Table 5 shows the number of predicted events by sample type, after tuning by the BANFF v5 ND280 fit.

4.3 SK 1R$_e$

This analysis uses SKMC v13a to generate the predicted spectra for the samples. The raw MC undergoes two tunings to generate the initial predicted distributions. First, the events are tuned according to the 11bv3.2 tuning including Run 4 data. Secondly, the events are tuned for the non-nominal values of the cross section parameters M_A^{RES}, CC1π E1, and NC1π0 according to a fit to the MiniBoone CC1π data as described in [5]. Table 6 gives the number of events in the 0–1250 MeV reconstructed energy range, broken down by sample type and interaction mode. Additionally, Table 7 shows the number of predicted events by sample type, after tuning by the BANFF v5 ND280 fit.

Table 8 shows the number of data events and predicted MC events and their ratios for the two samples, using PDG2012 values for the oscillation parameters; Figure 11 shows the same graphically as a function of E_{rec}, along with the unoscillated spectra. Figure 12 shows a scan of the total rates as a function of oscillation parameters.

Table 4: Top: Oscillated rates for $1R_\mu$, tuned by NIWG2012 for 6.57×10^{20} POT. Oscillation parameters used: $\sin^2\theta_{23} = 0.5$, $\sin^2\theta_{13} = 0.0251$, $\sin^2\theta_{12} = 0.311$, $\Delta m^2_{12} = 7.5\times10^{-5}$ eV, $\Delta m^2_{32} = 2.4\times10^{-3}$ eV, $\delta_{cp} = 0$. Bottom: Unoscillated rates for $1R_\mu$. All mixing angles set to zero.

	ν_μ	ν_e	$\bar{\nu_\mu}$	$\bar{\nu_e}$	$\nu_e$signal
CCQE	73.583	0.035	4.782	0.002	0.198
CC1π	41.398	0.029	2.949	0.002	0.081
CC coherent	0.897	0.001	0.247	0.000	0.005
CCnπ	6.558	0.004	0.404	0.000	0.001
CC other	2.175	0.003	0.100	0.000	0.001
NCπ^0	0.945	0.032	0.054	0.004	0.000
NC$\pi^{+/-}$	4.638	0.131	0.262	0.016	0.000
NC coherent	0.018	0.000	0.001	0.000	0.000
NC other	2.764	0.112	0.158	0.012	0.000
Sample Totals	132.977	0.348	8.956	0.036	0.285
Total Rate	142.603				

	ν_μ	ν_e	$\bar{\nu_\mu}$	$\bar{\nu_e}$	$\nu_e$signal
CCQE	367.066	0.038	9.710	0.002	0.000
CC1π	81.343	0.031	4.143	0.002	0.000
CC coherent	2.138	0.001	0.462	0.000	0.000
CCnπ	7.465	0.004	0.461	0.000	0.000
CC other	2.304	0.003	0.107	0.000	0.000
NCπ^0	0.945	0.032	0.054	0.004	0.000
NC$\pi^{+/-}$	4.638	0.131	0.262	0.016	0.000
NC coherent	0.018	0.000	0.001	0.000	0.000
NC other	2.764	0.112	0.158	0.012	0.000
Sample Totals	468.681	0.353	15.358	0.036	0.000
Total Rate	484.428				

Table 5: Top: Oscillated rates for 1R$_\mu$, tuned by BANFF2013 v5 for 6.57$\times 10^{20}$ POT. Oscillation parameters used: $\sin^2\theta_{23} = 0.5$, $\sin^2\theta_{13} = 0.0251$, $\sin^2\theta_{12} = 0.311$, $\Delta m^2_{12} = 7.5 \times 10^{-5}$ eV, $\Delta m^2_{32} = 2.4 \times 10^{-3}$ eV, $\delta_{cp} = 0$. Bottom: Unoscillated rates for 1R$_\mu$. All mixing angles set to zero.

	ν_μ	ν_e	$\bar{\nu_\mu}$	$\bar{\nu_e}$	$\nu_e$signal
Sample Totals	116.642	0.259	7.866	0.024	0.275
Total Rate	125.067				

	ν_μ	ν_e	$\bar{\nu_\mu}$	$\bar{\nu_e}$	$\nu_e$signal
Sample Totals	431.753	0.263	13.992	0.024	0.000
Total Rate	446.032				

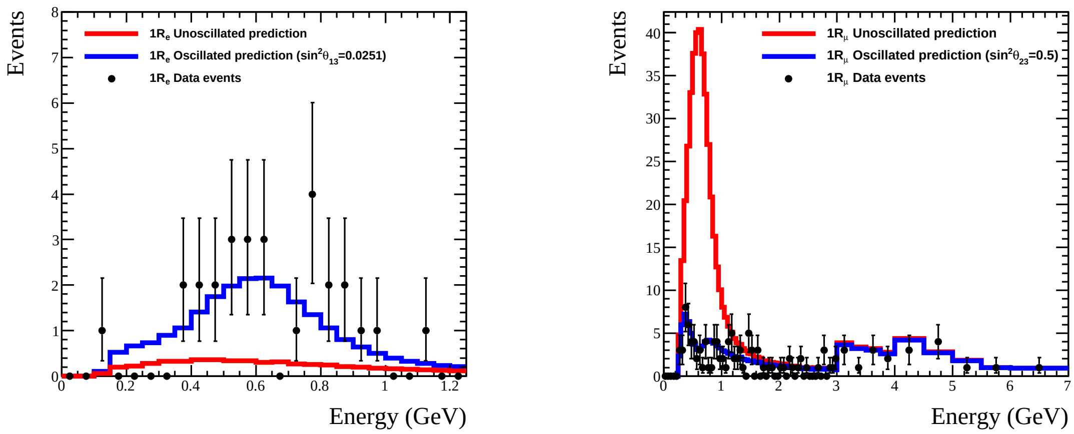

Figure 11: Oscillated (blue) and unoscillated (red) spectra for 1R$_\mu$ (left) and 1R$_e$ (right) samples. Rates are tuned by NIWG2012 for 6.57$\times 10^{20}$ POT. Oscillation parameters used: $\sin^2\theta_{23} = 0.5$, $\sin^2\theta_{13} = 0.0251$, $\sin^2\theta_{12} = 0.311$, $\Delta m^2_{12} = 7.5 \times 10^{-5}$ eV, $\Delta m^2_{32} = 2.4 \times 10^{-3}$ eV, $\delta_{cp} = 0$.

Table 6: Top: Oscillated rates for $1R_e$, tuned by NIWG2012 for 6.57×10^{20} POT, using the fiTQun π^0 cut. Oscillation parameters used: $\sin^2\theta_{23} = 0.5$, $\sin^2\theta_{13} = 0.0251$, $\sin^2\theta_{12} = 0.311$, $\Delta m^2_{12} = 7.5\times10^{-5}$ eV, $\Delta m^2_{32} = 2.4\times10^{-3}$ eV, $\delta_{cp} = 0$. Bottom: Unoscillated rates for $1R_e$. All mixing angles set to zero.

	ν_μ	ν_e	$\bar{\nu_\mu}$	$\bar{\nu_e}$	$\nu_e$signal
CCQE	0.050	2.276	0.001	0.098	14.989
CC1π	0.021	0.952	0.000	0.053	2.970
CC coherent	0.000	0.009	0.000	0.007	0.044
CCnπ	0.001	0.050	0.000	0.003	0.030
CC other	0.000	0.008	0.000	0.000	0.002
NCπ^0	0.475	0.015	0.024	0.002	0.000
NC$\pi^{+/-}$	0.149	0.004	0.008	0.000	0.000
NC coherent	0.181	0.005	0.016	0.001	0.000
NC other	0.329	0.010	0.013	0.001	0.000
Sample Totals	1.207	3.329	0.062	0.165	18.036
Total Rate	22.798				

	ν_μ	ν_e	$\bar{\nu_\mu}$	$\bar{\nu_e}$	$\nu_e$signal
CCQE	0.050	2.471	0.001	0.104	0.365
CC1π	0.021	1.010	0.000	0.056	0.040
CC coherent	0.000	0.010	0.000	0.007	0.001
CCnπ	0.001	0.052	0.000	0.003	0.000
CC other	0.000	0.008	0.000	0.000	0.000
NCπ^0	0.475	0.015	0.024	0.002	0.000
NC$\pi^{+/-}$	0.149	0.004	0.008	0.000	0.000
NC coherent	0.181	0.005	0.016	0.001	0.000
NC other	0.329	0.010	0.013	0.001	0.000
Sample Totals	1.206	3.585	0.062	0.175	0.406
Total Rate	5.434				

Table 7: Top: Rates for oscillated $1\mathrm{R}_e$ using the fiTQun π^0 cut and tuned by BANFF2013 v5 for 6.57×10^{20} POT. Oscillation parameters used: $\sin^2\theta_{23} = 0.5$, $\sin^2 2\theta_{13} = 0.1$, $\sin^2 2\theta_{12} = 0.8704$, $\Delta m^2_{12} = 7.6\times10^{-5}$ eV, $\Delta m^2_{32} = 2.4\times10^{-3}$ eV, $\delta_{cp} = 0$. Bottom: Rates for unoscillated $1\mathrm{R}_e$ using the fitqunπ^0 cut and tuned by BANFF2013 v5. Only $\sin^2 2\theta_{13} = 0.0$; other oscillation parameters remain the same.

	ν_μ	ν_e	$\bar{\nu_\mu}$	$\bar{\nu_e}$	$\nu_e$signal
Sample Totals	0.946	3.114	0.067	0.152	17.331
Total Rate	21.610				

	ν_μ	ν_e	$\bar{\nu_\mu}$	$\bar{\nu_e}$	$\nu_e$signal
Sample Totals	0.946	3.364	0.067	0.161	0.410
Total Rate	4.947				

Table 8: Number of data events in the SK samples, with MC tuned by NIWG2012 for 6.57×10^{20} POT, using the fiTQun π^0 cut for $1\mathrm{R}_e$. Oscillation parameters used: $\sin^2\theta_{23} = 0.5$, $\sin^2\theta_{13} = 0.0251$, $\sin^2\theta_{12} = 0.311$, $\Delta m^2_{12} = 7.5\times10^{-5}$ eV, $\Delta m^2_{32} = 2.4\times10^{-3}$ eV, $\delta_{cp} = 0$.

	$1\mathrm{R}_e$	$1\mathrm{R}_\mu$
Data	28	120
MC	22.798	142.603
Data/MC Ratio	1.228	0.841

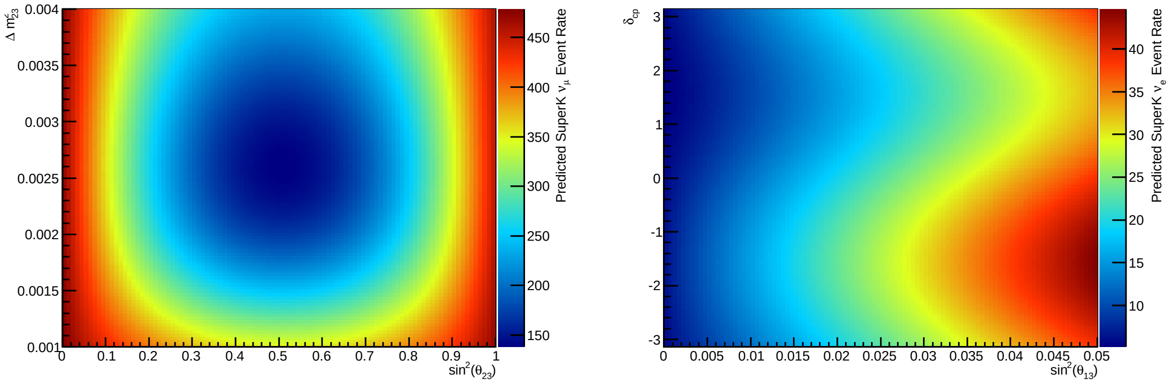

Figure 12: A scan of event rates for Run 1–Run 4 data of 6.57×10^{20} POT. Left shows $1\mathrm{R}_\mu$ scanning over $\sin^2\theta_{23}$ and Δm^2_{32}; right shows $1\mathrm{R}_e$ scanning over $\sin^2\theta_{13}$ and δ_{cp}. Other oscillation parameter are fixed at $\sin^2\theta_{23} = 0.5$ (for $1\mathrm{R}_e$), $\sin^2\theta_{13} = 0.0251$ (for $1\mathrm{R}_\mu$), $\sin^2\theta_{12} = 0.311$, $\Delta m^2_{12} = 7.5 \times 10^{-5}$ eV, $\Delta m^2_{32} = 2.4 \times 10^{-3}$ eV (for $1\mathrm{R}_e$), $\delta_{cp} = 0$ (for $1\mathrm{R}_\mu$)

5 Adaptive Kernel Density Method

The primary result of a Bayesian analysis such as this one is the whole posterior; however, it is desirable to summarize the result with a best fit point. Here, it is defined as the point of maximum probability density in oscillation parameter space. In the previous MCMC analysis, there were only two oscillation parameters of interest, and the best fit point was determined by the maximum bin of the binned 2D posterior in those parameters. This analysis, however, has four oscillation parameters of interest, and as a result, binning the posterior and finding the maximum bin quickly runs into a problem of bin statistics. Therefore, this analysis uses a kernel density estimation (KDE) technique to turn a set of discrete points into a smooth continuous density surface. Minuit [7] is then used to find the point of maximum density.

The kernel density estimator at a point x is defined as:

$$\hat{f}(x) = \frac{1}{nh}\sum_{i=1}^{n} K(\frac{x - x_i}{h}) \tag{3}$$

where x_1, x_2 ...x_n are discrete points and K is the kernel function. This analysis uses a gaussian kernel function, with bandwidth h becoming the σ of the gaussian:

$$\hat{f}(x) = \frac{1}{n}\sum_{i=1}^{n} \frac{1}{\sigma\sqrt{2\pi}} e^{-\left(\frac{x-x_i}{\sqrt{2}\sigma}\right)^2} \tag{4}$$

.

For optimum smoothing, we use an adaptive kernel density estimator that adjusts the bandwidth to the local density of points as detailed in [8]. In this method, the bandwidth is inversely proportional to the local density of points—producing a larger bandwidth in areas of low density and a smaller bandwidth in areas of high density—which means that low density areas are not undersmoothed and high density areas are not oversmoothed.

6 Fitter Validation

This analysis has been validated with three methods: using a nominal data set, an ensemble of toy experiments and a series of common fake data sets shared between joint oscillation analyzers.

6.1 Nominal Data Set

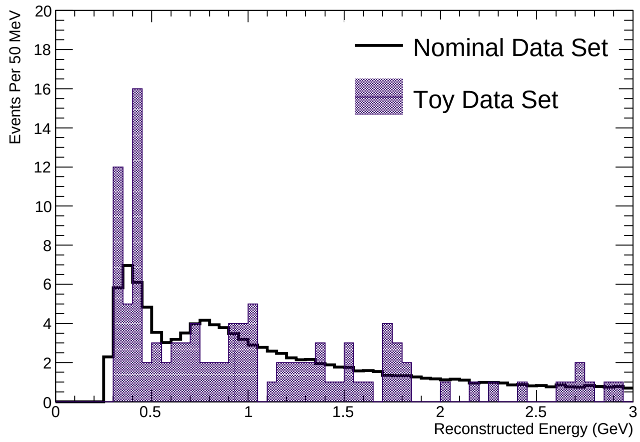

Figure 13: Nominal data set compared to a toy data set.

A nominal dataset is defined to be a toy experiment generated from the PDF in such a way that there are no statistical or systematic fluctuation as illustrated in Figure 13. This is achieved by reweighting the PDF to nominal values of systematic parameters, along with the chosen oscillation parameter values, and required protons on target, but instead of drawing randomly from the PDF, the PDF is considered as the dataset. This produces a dataset free from statistical fluctuations, which, when fit, should result in parameters free from bias. Figures 14 and 15 show the results of a fit to a nominal dataset using 20 million MCMC steps. Figure 14 shows the best fit values of all systematic parameters and their posterior error, and Figure 15 shows the fractional residual of each systematic parameter. Both plots show minimal bias in the parameters, and are complimentary to the toy experiment results in section 6.2.

Figures 16 and 17 show credible intervals and best fit values constructed from the nominal posterior distributions. Also plotted are the true parameter values of the nominal data set.

6.2 Toy Experiments

Toy experiments are produced by throwing fake datasets from both SK and ND280 PDFs. Data sets are generated from poisson fluctuations of a particular underlying

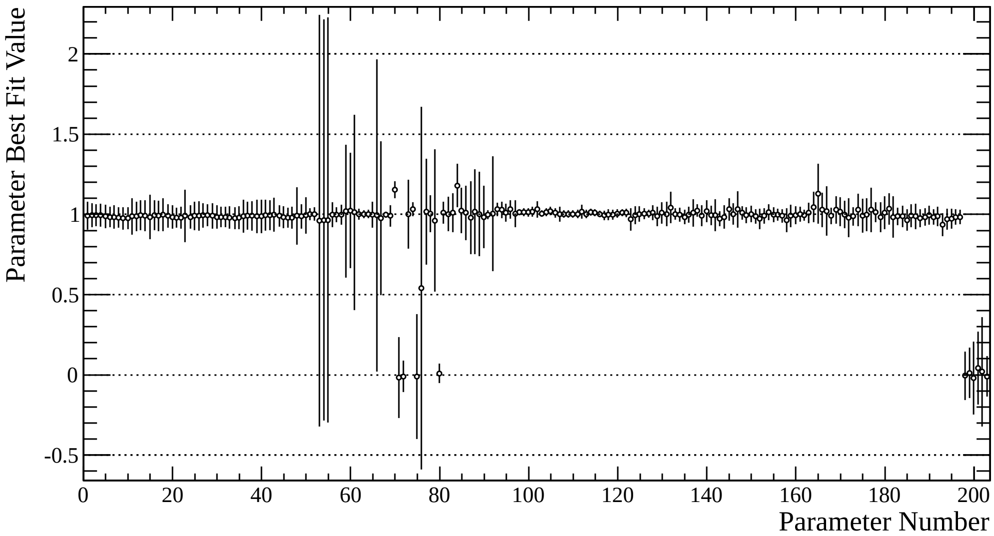

Figure 14: Nominal best fit values from systematic parameters. Error bars are the posterior error. Most parameters have either a true central value of 1 or 0.

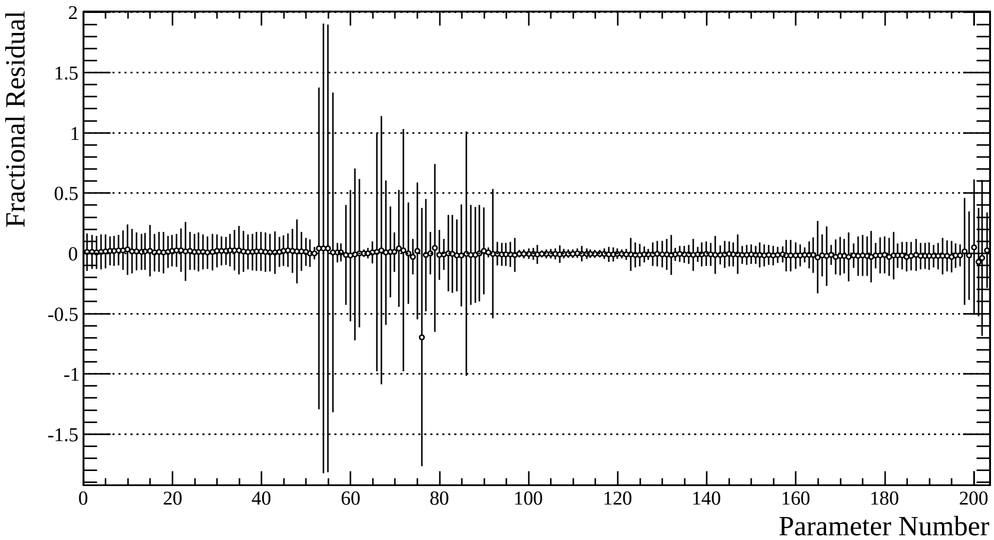

Figure 15: Nominal best fit value subtracted from the true central value, divided by the best fit value. Shows the fractional shift from the true value of each systematic parameter. All parameters stay within 10% of the true value.

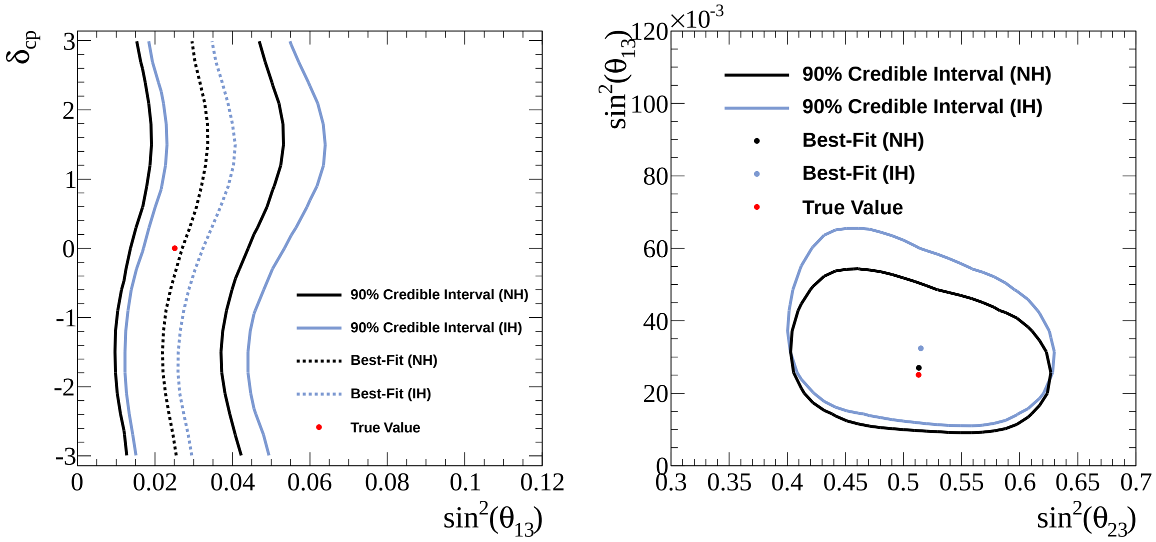

(a) (b)

Figure 16: Nominal data fit contours. In (a), best fit lines are constructed in slices of δ_{cp}, and the value at $\delta_{cp} = 0$ is positively offset from the true value due to marginalization of the spectral function as shown in Figure 21.

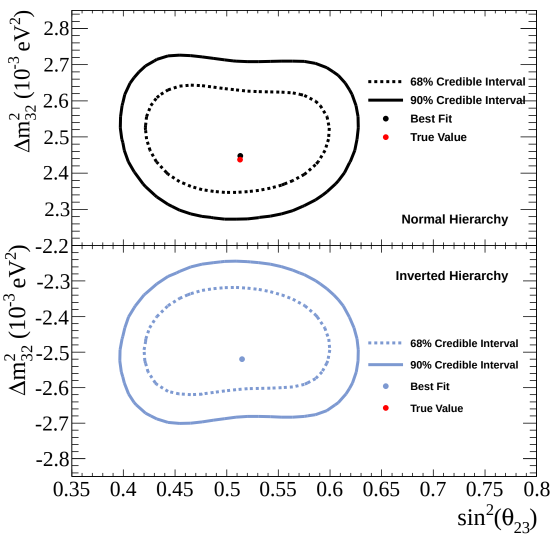

Figure 17: $\sin^2(\theta_{23})$ vs Δm^2_{32} separated into both hierarchies for a nominal data fit.

PDF. To create this underlying PDF, all systematic parameters are kept at nominal values; however, systematic fluctuation is introduced by randomly throwing the central values for the systematic penalty terms when performing the fit. In Equation 5, p^{nom} is the central value which is thrown separately for each toy dataset, according to the prior PDF for that systematic, including the correlation between related systematics. Toy experiments are fit using a minimum of 10^6 steps to allow the production of many fits, whilst ensuring adequate convergence.

$$-\ln P = \sum_{i=0}^{n}\sum_{j=0}^{n}\frac{1}{2}(p_i^{prop} - p_i^{nom})V_{ij}^{-1}(p_j^{prop} - p_j^{nom}) \tag{5}$$

To test the fitter for bias and correct error determination, the following definition is used to construct pull distributions for all parameters:

$$pull = \frac{\mu_{fit} - \mu_{true}}{\sigma_{fit}} \tag{6}$$

The best fit and post-fit error for nuisance parameters are extracted from the toy posterior distributions by constructing a 1D marginal distribution for each parameter and fitting a gaussian to a restricted range defined by $\mu \pm rms$ of the histogram. For oscillation parameter pulls, the best fit is found using the 3D posterior mode at $\delta_{cp} = 0$ described in Section 5. Because the 1D posterior distributions for the oscillation parameters are non-gaussian, the RMS is used as a better estimate of the error.

The post-fit error σ_{fit} of each parameter for every toy experiment was plotted against the prior error and, where available, the ND280 BANFFv2 post-fit error value [9] in Figure 18. Shown in Figure 19 is the mean of the pull distributions for the toys, constructed from Equation 6. The plots in Figure 20 show the oscillation parameter pull distributions.

6.3 Marginalization Induced Biases

To extract the best fit values and errors necessary for pull calculations, the 1D marginal posterior for each parameter is constructed as described in section 6.2. This method means that for each parameter, the best fit estimate and error is found marginalizing all other parameters. In doing so, any non-gaussian behavior and correlations with parameters with non-gaussian behavior can cause apparent

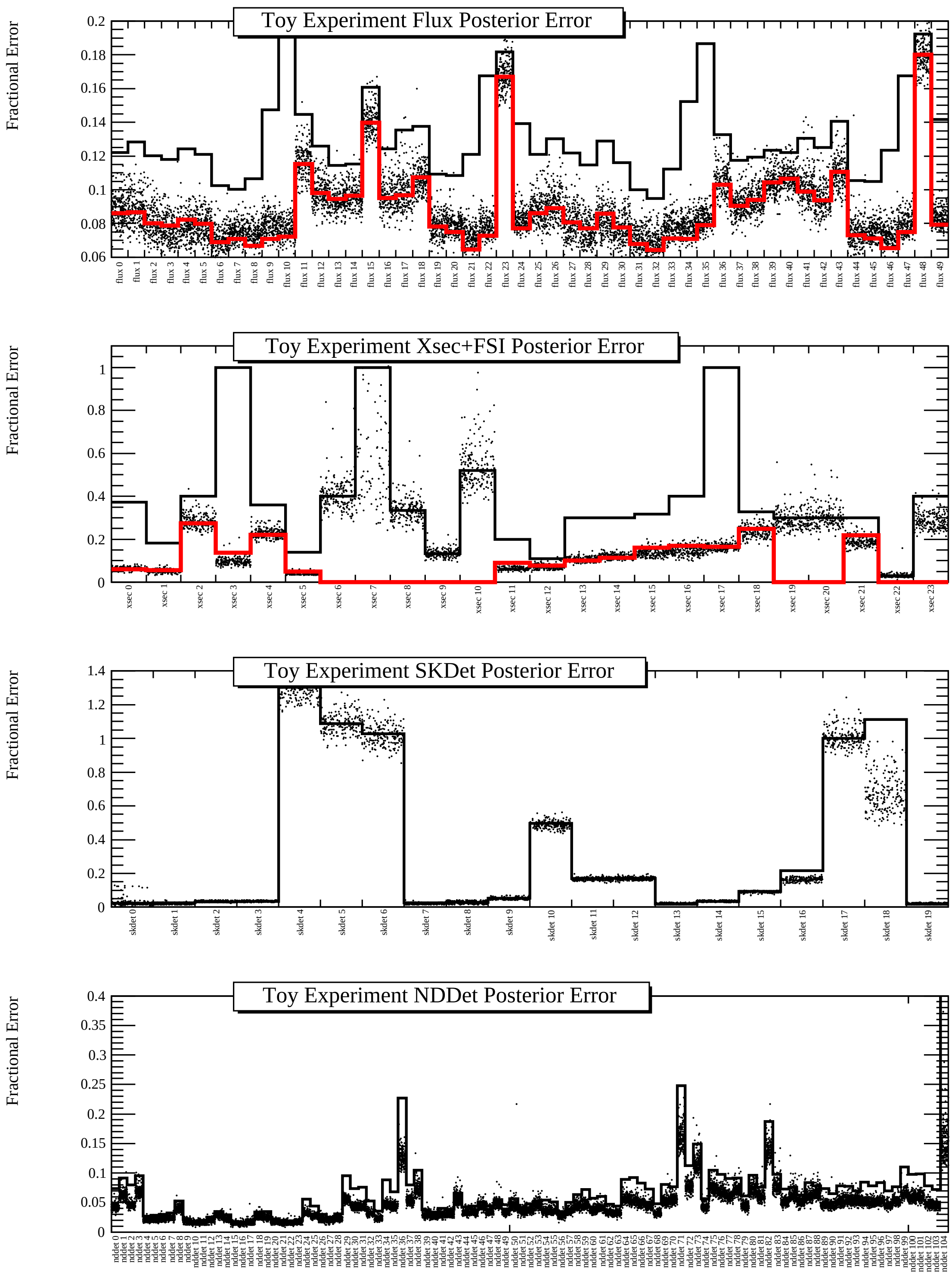

Figure 18: Black line: prior error on parameter. Red line: BANFFv2 post-fit error (where applicable). Black points: posterior error from toy experiments. These plots show how the power to constrain parameter errors is in good agreement with the BANFFv2 post-fit values.

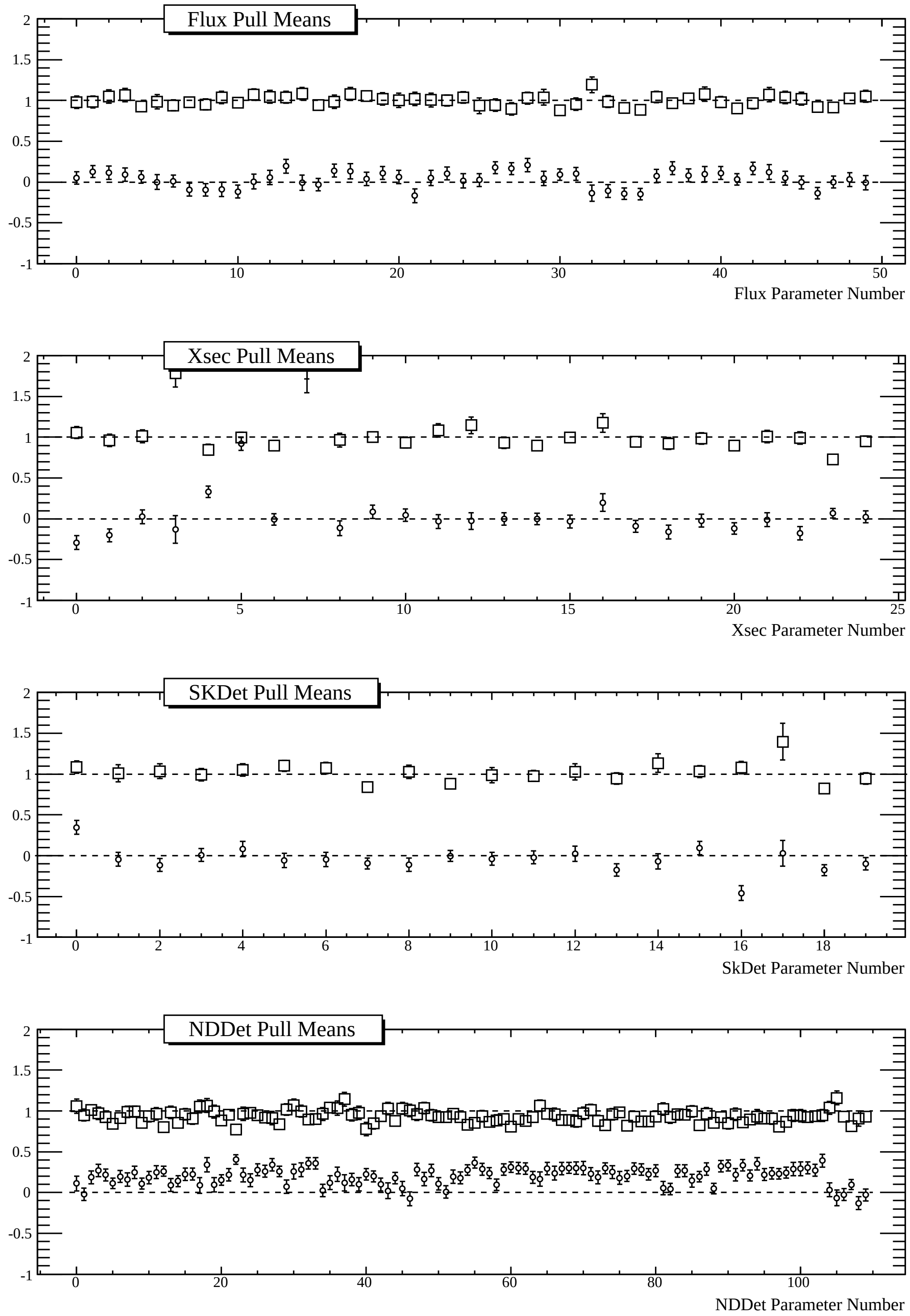

Figure 19: Pull means

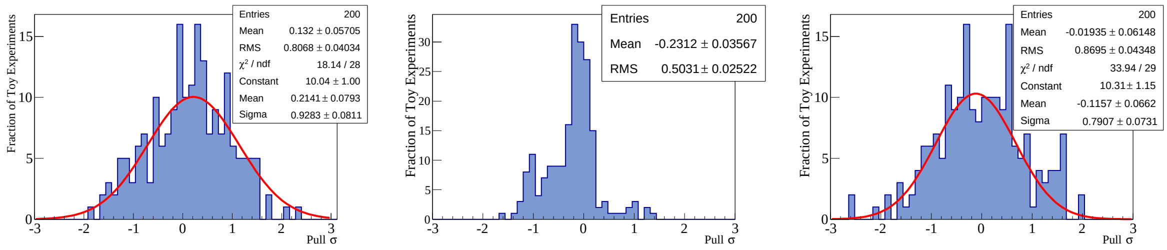

(a) $\sin^2(\theta_{13})$ pull distribution (b) $\sin^2(\theta_{23})$ pull distribution (c) Δm^2_{32} pull distribution

Figure 20: Oscillation parameter pulls for $\delta_{cp} = 0$. Since there is no sensitivity to fit for δ_{cp}, the pull distribution is omitted.

biases in the mean of the pull distributions. In this analysis, there are several parameter pulls which are not within 1σ of 0. These are:

- Quasi-Elastic Axial Mass (M_A^{QE}): this parameter is correlated with the ND280 spectral function parameter, which is both non-gaussian and one-sided (Figure 22).
- Fermi momentum: this parameter is highly correlated with spectral function, which likewise produces an apparent shift as with M_A^{QE}. (Figure 23).
- Spectral function for carbon and oxygen: these are parameters which are defined to be between 0 and 1, and have a distinctly non-gaussian shape in the posteriors.
- SK Energy Scale: the energy scale is a unique parameter in that it shifts the reconstructed energy of events from both SK samples. A high enough shift will cause an event to migrate to an adjacent bin. This behavior causes a non-gaussian posterior distribution for the energy scale parameter. Although the posterior mode shows there is negligible bias, fitting a gaussian to a non-gaussian distribution causes a bias in the resulting pull distribution (Figure 24).
- CCnQE ν_μ Normalization: this parameter is correlated with the oscillation parameters. Since these parameters have non-gaussian posterior distributions, marginalizing them affects the posteriors of correlated parameters. This manifests in the CCnQE ν_μ normalization parameter as a small negative shift in the central value.

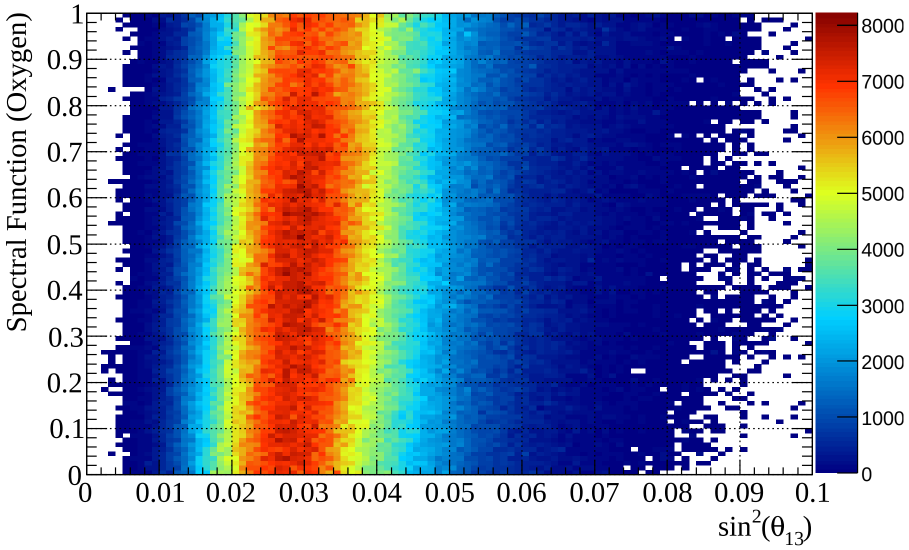

Figure 21: Joint posterior for $\sin^2(\theta_{13})$ and the oxygen spectral function. When marginalizing the spectral function, due to the correlations between both parameters and the boundary at 0, a shift in probability to positive values is caused in the 1D marginal posterior of $\sin^2(\theta_{13})$. Plot constructed from a nominal data set posterior.

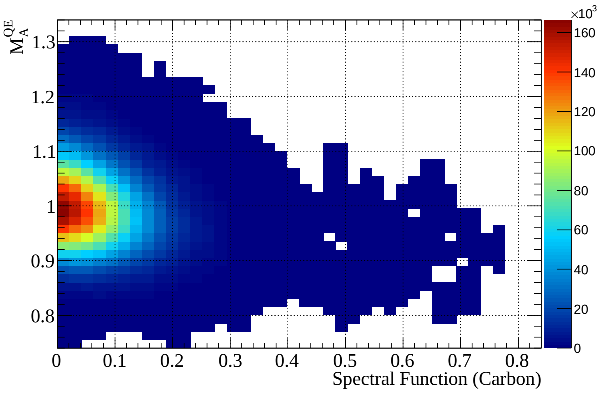

Figure 22: Correlation between quasi-elastic axial mass and spectral function parameters for carbon. Plot constructed from a nominal data set posterior.

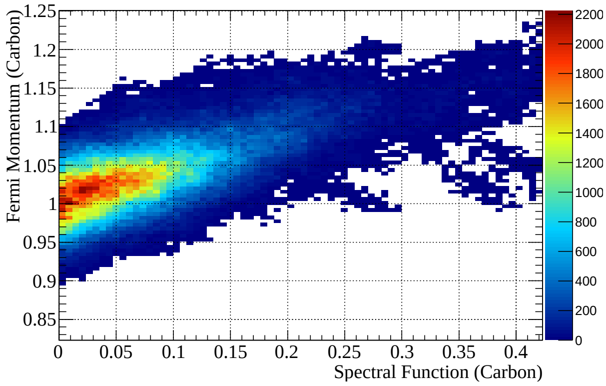

Figure 23: Correlation between fermi momentum and spectral function parameters for carbon. Plot constructed from a nominal data set posterior.

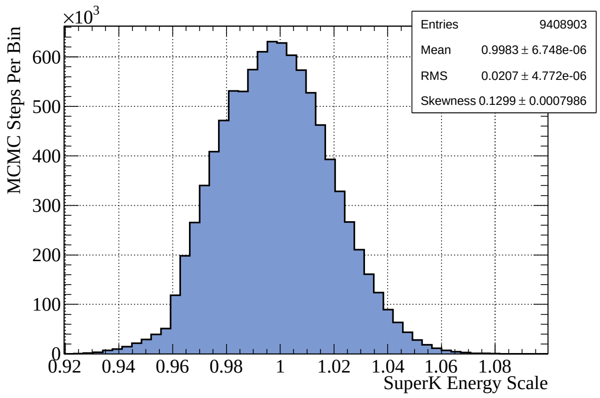

Figure 24: Non-gaussian posterior distribution of the SK energy scale parameter. Plot constructed from a nominal data set posterior.

6.4 Fake Data Set Fits

A series of 6 fake data sets (FDS) were produced by the VaLOR group and distributed to the joint oscillation analyzers. The parameter values used to generate these data sets are denoted in Table 9. Best-fit points for T2K only fits are found using the adaptive kernel density estimator method with δ_{cp} fixed at the VALOR best fit value. When including the reactor constraint, the best fit is found in 4 dimensions. The $\sin^2(\theta_{13}) - \delta_{cp}$ best fit line is drawn for fits without reactor constraint. It is constructed by finding the maximum density in 3D for steps along the δ_{cp} posterior.

Table 9: Table showing the configuration of the fake data sets provided by the VaLOR group. **Bold** elements highlight the defining parameter value of that data set.

Fake Data Set	Mass Hierarchy	$\sin^2(\theta_{23})$	Δm^2_{32}	$\sin^2(\theta_{13})$	δ_{cp}	Systematic
0	NH	0.513	2.4375	0.0251	0	Nominal
1	NH	**0.37**	2.4375	0.0251	0	Random Throws
2	NH	0.513	**2.75**	0.0251	0	Random Throws
3	NH	0.513	2.4375	**0.04**	0	Random Throws
4	NH	0.513	2.4375	0.0251	$\boldsymbol{-\pi/2}$	Nominal
5	**IH**	0.513	2.4375	0.0251	0	Nominal

6.4.1 T2K Only Fits

One example of the 2D contours in $\sin^2(\theta_{23})$–Δm^2_{32} and $\sin^2(\theta_{13})$–δ_{cp} is shown in Figure 25. The contours for all other datasets are contained in Appendix A. There is generally good agreement between the two fitters, and between the fitters and the input values, as shown in Table 10. Generally, the MaCh3 fitter finds a higher value of $\sin^2(\theta_{13})$ than the VaLOR fit; this difference is consistent with the size of shifts coming from the marginalization over spectral function.

There is an interesting discrepancy between the two fitters in FDS1, where the input value was an off-maximal value of $\sin^2\theta_{23} = 0.37$. MaCh3 finds the best fit value in the lower octant, where VaLOR finds the best fit value in the upper octant. This discrepancy is explained in Figure 26, which shows the full marginal posterior in $\sin^2\theta_{23}$, and there is greater posterior density in the lower octant. However, if plots/fds/fds_1_cont_th23dm23-eps-converted-to.pdf

(a) 1Rν_μ

plots/fds/fds_1_cont_th13dcp-eps-converted-to.pd

(b) 1Rν_e

Figure 25: Fake Data Set 1

the posterior is restricted to a smaller window around the best fit points in $\sin^2\theta_{13}$ and Δm^2_{32}—a technique similar to the profiling method of the minimizer fit—there is greater posterior density in the upper octant. Thus, the difference in the best fit points comes from the difference in the methods of the fitters.

plots/fds/fds1_diff-eps-converted-to.pdf

Figure 26: The full marginal posterior of $\sin^2(\theta_{23})$ for FDS1 (cyan) compared with a "restricted posterior" constructed from MCMC steps taken only from a small region around the best fit point of $\sin^2(\theta_{13})$ and Δm^2_{32} (darker blue). Restricting the posterior to points only around the most probable regions of the marginalized oscillation parameters is similar in approach to the frequentist profiling technique. Red arrows indicate the 1D posterior mode for each distribution. This exercise highlights the difference in best fit points between analyses.

Table 10: Normal hierarchy best-fit comparison table between MaCh3 and VaLOR for all fake data sets with no reactor constraint. MaCh3 values of Δm^2_{32} have been rescaled to enable comparison with the Fogli convention used by VaLOR.

FDS	$\Delta m^2_{32} \times 10^{-3}$	$\sin^2(\theta_{23})$	$\sin^2(\theta_{13})$	δ_{cp}
0 True	**2.4375**	**0.513**	**0.0251**	**0**
0 VALOR	2.413	0.513	0.0364	-0.0825
0 MaCh3	2.419	0.522	0.0385	-0.0825
1 True	**2.4375**	**0.37**	**0.0251**	**0**
1 VALOR	2.327	0.619	0.0152	1.585
1 MaCh3	2.268	0.409	0.0259	1.585
2 True	**2.75**	**0.513**	**0.0251**	**0**
2 VALOR	2.578	0.508	0.0185	-0.0179
2 MaCh3	2.598	0.508	0.0200	-0.0179
3 True	**2.4375**	**0.513**	**0.04**	**0**
3 VALOR	2.583	0.568	0.0572	1.087
3 MaCh3	2.578	0.535	0.0642	1.087
4 True	**2.4375**	**0.513**	**0.0251**	**0**
4 VALOR	2.466	0.526	0.0464	-2.564
4 MaCh3	2.468	0.526	0.0494	-2.564
5 True	**2.4375**	**0.513**	**0.0251**	**0**
5 VALOR	2.53	0.511	0.0246	2.367
5 MaCh3	2.56	0.511	0.0232	2.367

6.4.2 T2K with Reactor Constraint

The application of a prior constraint from reactor experiments can provide increased sensitivity to the oscillation parameters. For these toy datasets, the constraint was applied as the true input $\sin^2 2\theta_{13}$ constraint, ± 0.01, the PDG 2013 error. Figure 27 shows one example of this process, for FDS 0. The plots for the other FDS are in Appendix A.

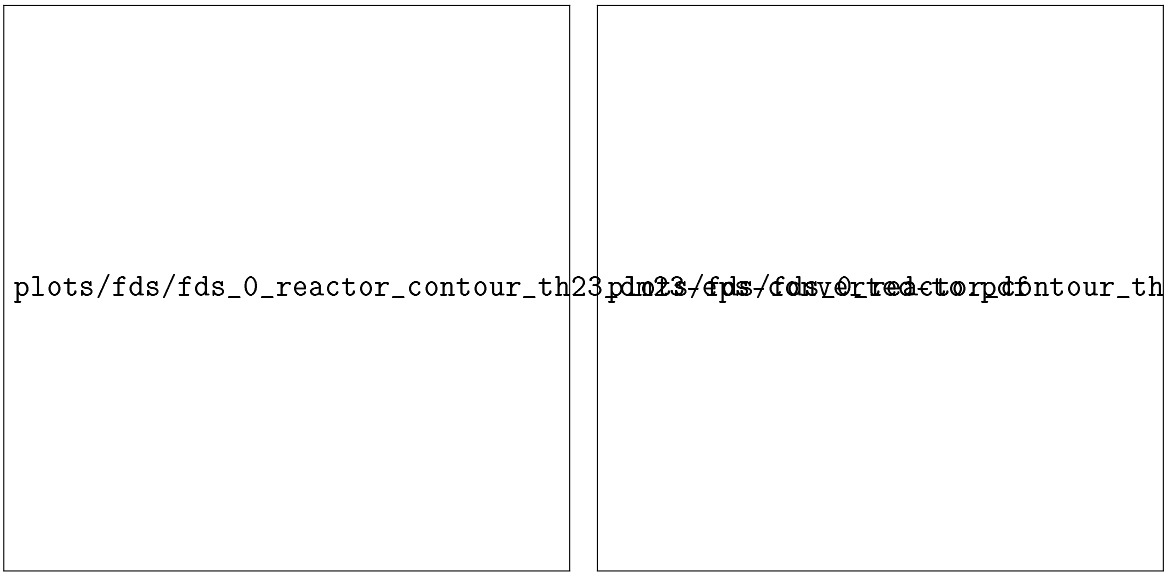

(a) $1\text{R}\nu_\mu$

(b) $1\text{R}\nu_e$

Figure 27: Fake Data Set 0

6.5 Comparison with BANFF Matrix Fit

The fitter can also be configured to constrain the SK flux and cross-section uncertainties using the BANFF matrix instead of using the ND280 data directly. A comparison of the contours and best fit points (Figure 28) produced with both methods when fitting fake data set 5 was made and the results show negligible difference between the two results.

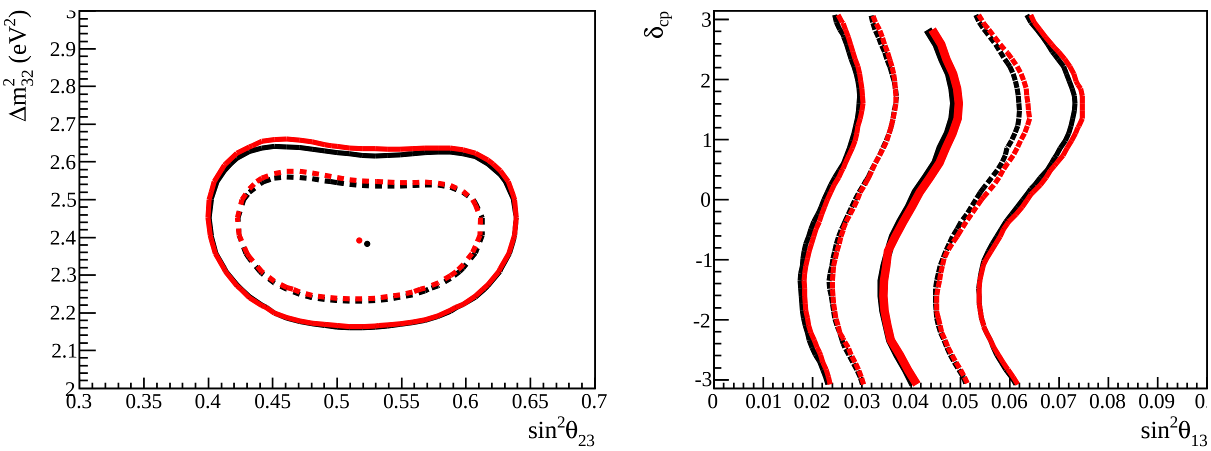

Figure 28: The comparison of contours and best fit points between the BANFF extrapolation (red) and the simultaneous fit with ND280 data methods. The contours suggest that the simultaneous fitting method yields a smaller uncertainty, however the difference is considered negligible.

7 Fit Results

This section details the results obtained from fitting simultaneously the SK and ND280 Run 1–4 data, totalling 6.57×10^{20} and 5.9×10^{20} protons on target respectively. For these fits, the solar sector oscillation parameters are $\sin^2\theta_{12} = 0.311 \pm 0.017$ and $\Delta m^2_{21} = 7.5 \pm 0.2 \times 10^{-5}$ eV^2.

7.1 T2K Run 1–4 Data Fit

The data samples were first fit using T2K data alone, with a Markov chain of 1.8×10^7 steps after burn-in. For this type of fit, since there is little constraint in δ_{cp}, the best fit point is found by fixing δ_{cp} at 21 steps in its range, and fixing the parameter in the 4D adaptive kernel estimation to find the best fit in 3D for the other oscillation parameters. Table 11 shows the best fit parameters in the $\delta_{cp} = 0$ slice. Credible regions are produced in 2D for several different sets of parameters; these contours are produced marginalized over all other parameters, but constructed separately for normal and inverted hierarchies. Figure 7.1 shows the contours in $\sin^2(\theta_{23})$–Δm^2_{32} space. Figure 30(a) shows the contours in $\sin^2(\theta_{13})$–δ_{cp} space, where the best fit is shown as a line connecting the best fit values in the slices of δ_{cp}. Figure 30(b) shows the contours in $\sin^2(\theta_{23})$–$\sin^2(\theta_{13})$.

Figure 31 shows the 1D credible intervals for $\sin^2(\theta_{13})$, $\sin^2(\theta_{23})$, and Δm^2_{32}, where all other parameters are marginalized.

Figure 7.1 shows the best fit spectra of the Run 1–4 SK data constrained by the ND280 data, for 1R$_\mu$ and 1R$_e$ samples. The best fit spectra is determined via a marginalization method. The fit posterior is sampled randomly 2500 times, and with each sample the parameter values are used to calculate the expected event rate per bin of the energy spectra; this is essentially marginalizing over all parameters, oscillation included, to find the posterior distribution in each energy bin. The combination of all the samples creates a distribution of event rates for each bin. Finally, for each bin, a gaussian is fitted around the peak of the event rate distribution, and the mean of the fit is taken to be the predicted value for that bin. Most bins take on a gaussian shape, but in some bins, especially near the oscillation maxima in the 1R$_\mu$ sample, the distribution is non-gaussian, due to the influence of the nearby physical boundary in $\sin^2\theta_{23}$.

Table 11: Best-fit values for oscillation parameters extracted from the marginal posterior of the Run 1–4 data.

	$\lvert\Delta m^2_{32}\rvert$	$\sin^2(\theta_{23})$	$\sin^2(\theta_{13})$	δ_{cp}
Normal Hierarchy	2.491	0.520	0.0377	0 (fixed)
Inverted Hierarchy	2.571	0.520	0.0454	0 (fixed)

plots/rdf/contour_th23_dm23-eps-converted-to.pdf

Figure 29: Run 1–4 data fit 2D contours in $\sin^2(\theta_{23})$–Δm^2_{32} space.

plots/rdf/contour_th13_dcp-eps-conve plots/rdf/contour_th23_th13-eps-converted-to.pd

(a) (b)

Figure 30: Run 1–4 data fit 2D contours in (a) $\sin^2(\theta_{13})$–δ_{cp} space and (b) $\sin^2(\theta_{23})$–$\sin^2(\theta_{13})$ space.

Figures 33 and 34 show the momentum and angle distributions for ND280 with the pre-fit MC prediction and post-fit spectra, calculated in the same way as for the SK spectra.

A goodness-of-fit is calculated as in [?], where at each chain sample used for the best fit spectra, a fake dataset is thrown from the MC prediction for that sample. The log likelihood ratio between the fake dataset and the MC prediction is calculated, as is the log likelihood ratio between the real data and the MC prediction. A p-value is calculated as the percentage of samples for which the data better fit the MC prediction than the fake data. In order to have $N > 10$ in each bin, a requirement for this method, the 1R$_\mu$ sample is rebinned into five bins (0–0.4; 0.4–0.7; 0.7–1.0; 1.0–2.0; and 2.0–30.0 GeV) and the 1R$_e$ sample is considered as one bin only. The ND280 sample is considered in the bins used to fit the data. This means that the overall p-value is completely dominated by the ND280 sample. Figure 35 shows the ND280, 1R$_\mu$, 1R$_e$, and total distributions for the quantity $\ln L_{data} - \ln L_{throw}$; the p-value is the percentage of this distribution above zero. The p-values are: ND280-only, 0.044; SK 1R$_e$, 0.32; SK 1R$_\mu$, 0.35; and all samples, 0.036. These values indicate no disagreement with data for the SK samples. The value for plots/rdf/CredibleIntervals1D-eps-converted-to.pdf

Figure 31: Credible intervals in 1D for $\sin^2(\theta_{13})$, $\sin^2(\theta_{23})$, and $|\Delta m^2_{32}|$. The PDFs for the angles are shown for normal hierarchy, inverted hierarchy, and marginalized over the hierarchies. The PDF for the mass splitting is shown only for normal and inverted hierarchies. The 90% credible intervals are shown by the dotted lines and given in the plot legends.

plots/rdf/bfs_rdf1_t2konly-eps-converted-to.pdf

Figure 32: Run 1–4 data best fit spectra for SuperK $1R_{\mu}$ and $1R_{e}$ samples.

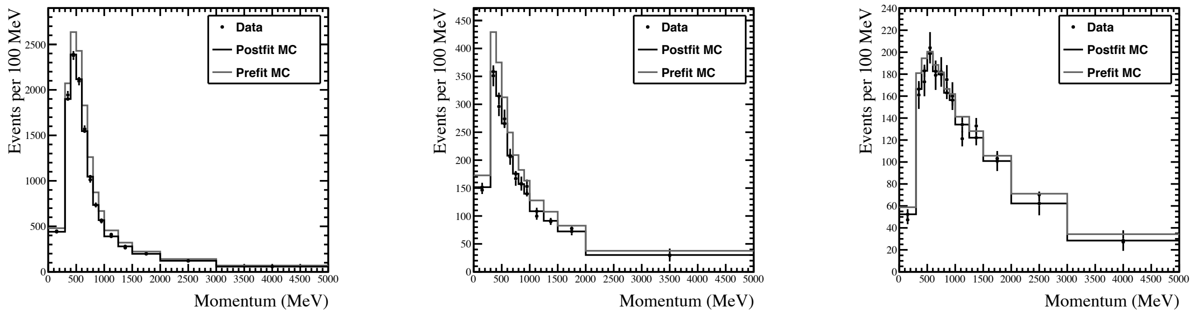

Figure 33: The data (black points) and pre-fit (grey) and post-fit (black) predicted number of MC events projected onto the momentum axis. Shown left-to-right are the CC0π sample, the CC1π sample, and the CCoth sample.

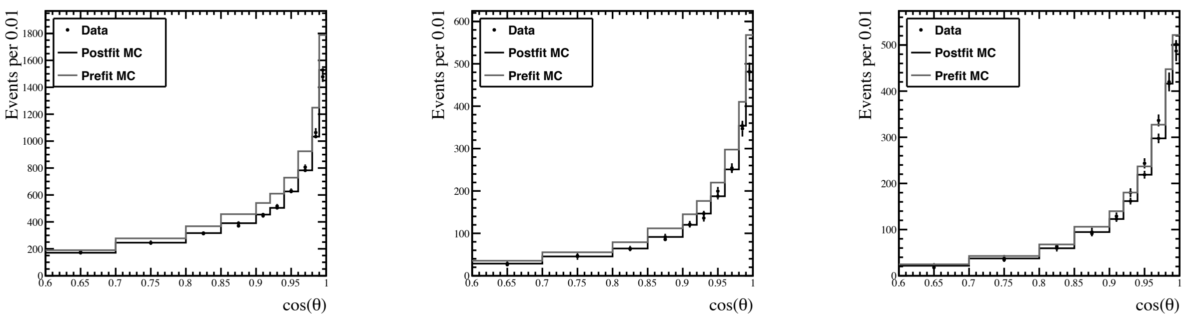

Figure 34: The data (black points) and pre-fit (grey) and post-fit (black) predicted number of MC events projected onto the $\cos\theta$ axis. Shown left-to-right are the CC0π sample, the CC1π sample, and the CCoth sample.

the ND280 samples is somewhat low, indicating some disagreement; however, this is a known effect (see [9]), and the agreement between the results of the ND280 fits for both MaCh3 and the minimizer BANFFv2 fit and the data are nearly equivalent.

plots/rdf/GOF-eps-converted-to.pdf

Figure 35: Goodness-of-fit distributions for the three different samples in the fit and the summed total. The p-value is the percentage of each distribution which is greater than zero.

7.2 T2K Run 1–4 Data Fit With Reactor Constraint

The data samples were then fit using T2K data in combination with the PDG 2013 reactor gaussian constraint of $\sin^2(2\theta_{13}) = 0.095 \pm 0.01$, with a Markov chain of 3.168×10^7 steps after burn-in. For this type of fit, the best fit point is found with a 4D adaptive kernel estimate of the oscillation parameters of interest. Table 12 shows the best fit parameters. Credible regions are produced in 2D for several different sets of parameters; these contours are produced marginalized over all other parameters, but constructed separately for normal and inverted hierarchies. Figure 36 shows the contours in $\sin^2(\theta_{23})$–Δm^2_{32} space. Figure 37(a) shows the contours in $\sin^2(\theta_{13})$–δ_{cp} space. Figure 37(b) shows the contours in $\sin^2(\theta_{23})$–$\sin^2(\theta_{13})$.

Figure 38 shows the 1D credible intervals for $\sin^2(\theta_{13})$, $\sin^2(\theta_{23})$, and Δm^2_{32}, where all other parameters are marginalized.

Table 12: Best-fit values for oscillation parameters extracted from the marginal posterior of the Run 1-4 data fit with reactor constraint.

	$\lvert\Delta m^2_{32}\rvert$	$\sin^2(\theta_{23})$	$\sin^2(\theta_{13})$	δ_{cp}
Normal Hierarchy	2.510	0.527	0.0247	-1.551
Inverted Hierarchy	2.553	0.531	0.0249	-1.596

plots/rdf/reactor_contour_th23_dm23-eps-converted-to

Figure 36: Run 1–4 data fit with reactor constraint 2D contours in $\sin^2(\theta_{23})$–Δm^2_{32} space.

The goodness-of-fit was repeated for the reactor constrained data. Figure 41 shows the ND280, 1R$_\mu$, 1R$_e$, and total distributions for the quantity $\ln L_{data} - \ln L_{throw}$; the p-value is the percentage of this distribution above zero. The p-values are: ND280-only, 0.044; SK 1R$_e$, 0.44; SK 1R$_\mu$, 0.33; and all samples, 0.042. These values indicate no disagreement with data for the SK samples. It is interesting that the p-value for SK 1R$_e$ increases slightly for this fit as compared to the T2K-only fit, despite the fact that the predicted number of events for the T2K-only fit is closer to the number of data events. This is due to the fact that the reactor constraint

(a) 1Rν_e (b) 1Rν_μ

Figure 37: Run 1-4 data fit with reactor constraint 2D contours in (a) $\sin^2(\theta_{13})$–δ_{cp} space and (b) $\sin^2(\theta_{23})$–$\sin^2(\theta_{13})$ space.

narrows the distribution of allowed events significantly, and therefore the predicted spectra from the throws do not move as far from the data point as they do for the T2K-only fit.

The addition of the reactor constraint to the T2K data also produces some sensitivity in δ_{cp}. Figure 42 shows the δ_{cp} posterior for the normal hierarchy, considered alone; the inverted hierarchy, considered alone; and marginalizing over the hierarchies. Figure 43 shows the δ_{cp} posterior when considering the normal and inverted hierarchies jointly. Each of these methods answers a slightly different question about the preferred region for the value of δ_{cp}, and caution should be used when using these plots to describe them correctly. Table 13 enumerates the 90% allowed regions for the different methods.

The constraint on δ_{cp} can also be considered separating the lower and upper octant, as in Figure 4 of [?]. This is shown in Figure 44. Unlike the MINOS data, the best fit point remains constant at $\approx -\pi/2$ for all of the choices of octant and hierarchy. However, some are more preferred than others; the inverted hierarchy/lower octant choice is excluded completely at the 68% level and nearly completely at the 90% level. By contrast, nearly all of the normal hierarchy/upper octant is allowed plots/rdf/CredibleIntervals1DReactor-eps-converted-to.pdf

Figure 38: Credible intervals in 1D for $\sin^2(\theta_{13})$, $\sin^2(\theta_{23})$, and $|\Delta m^2_{32}|$, using the reactor constraint. The PDFs for the angles are shown for normal hierarchy, inverted hierarchy, and marginalized over the hierarchies. The PDF for the mass splitting is shown only for normal and inverted hierarchies. The 90% credible intervals are shown by the dotted lines and given in the plot legends.

plots/rdf/bfs_rdf1_reactor-eps-converted-to.pdf

Figure 39: Run 1–4 data best fit spectra for SuperK ν_μ and ν_e samples with reactor constraint.

plots/rdf/bfs_overlay-eps-converted-to.pdf

Figure 40: Comparison of best fit spectra of T2K data with and without reactor constraint applied.

plots/rdf/GOF_R-eps-converted-to.pdf

Figure 41: Goodness-of-fit distributions for the three different samples in the fit and the summed total. The p-value is the percentage of each distribution which is greater than zero.

plots/rdf/dcp_marg-eps-converted-to.pdf

Figure 42: The posterior probability for δ_{cp}, marginalized over all other parameters. The red curve shows the posterior for the normal hierarchy only; the blue curve for the inverted hierarchy only; and the black curve marginalized over the hierarchies. The grey bands show the 68% and 90% credible intervals for the posterior marginalized over δ_{cp}.

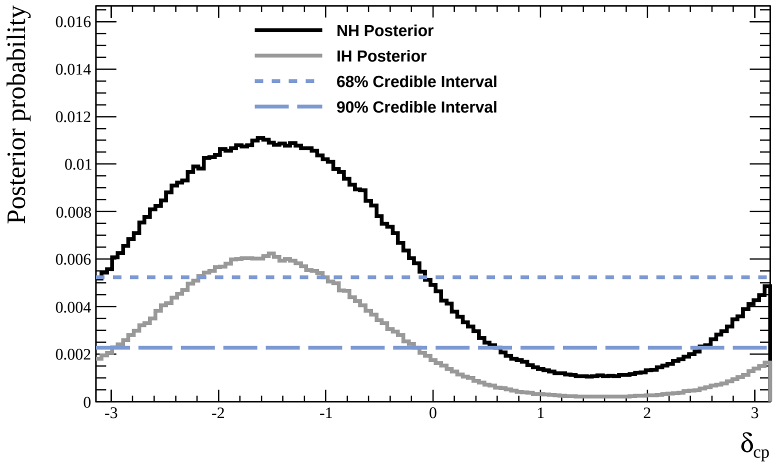

Figure 43: The posterior probability for δ_{cp}, for the normal and inverted hierarchies considered jointly. The dotted lines show the 68% and 90% credible intervals, where the allowed region is the region of the posterior above the line.

at the 90% level.

Table 13: The 90% allowed credible interval for different methods of constructing the δ_{cp} posterior.

Method	90% Allowed Credible Interval
Normal Hierarchy ONLY	$[-\pi, 0.45] \cup [2.66, \pi]$
Inverted Hierarchy ONLY	$[-\pi, 0.15] \cup [3.04, \pi]$
Marginalized Hierarchy	$[-\pi, 0.38] \cup [2.79, \pi]$
Joint Hierarchy	$[-\pi, 0.68]$ (NH) $\cup [2.49, \pi]$ (NH) $\cup [-2.99, -0.08]$ (IH)

The Markov chain also provides an interesting and natural way to compare the mass hierarchies. Figure 45 shows the 1D posterior for Δm^2_{32}. In this framework, the integral of posterior where $\Delta m^2_{32} > 0$ gives the probability that the true hierarchy is normal; for this analysis, that probability is 69.1%, or about a 2.24:1 preference of the data for the normal hierarchy. This is interesting, but not significant enough to draw any firm conclusions. A similar number can be produced for the preference of $\sin^2(\theta_{23}) > 0.5$ or < 0.5; the data prefers $\sin^2(\theta_{23}) > 0.5$ at 2.87:1. Again,

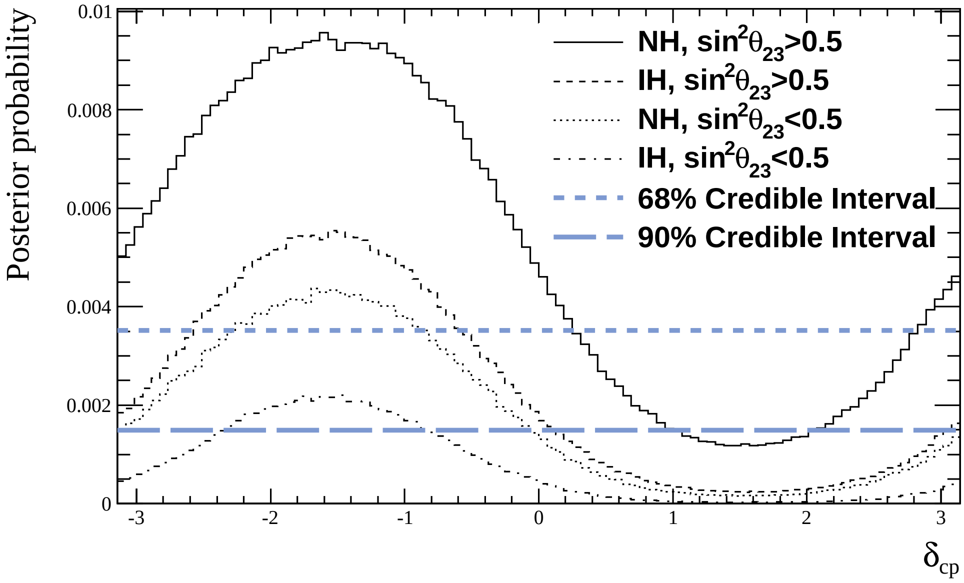

Figure 44: The marginalized δ_{cp} posteriors, for normal and inverted hierarchies, as well as $\sin^2\theta_{23} > 0.5$ or < 0.5. The four choices are considered jointly for setting the credible interval levels. The allowed region is the region of the posterior above the line.

interesting, but not significant.

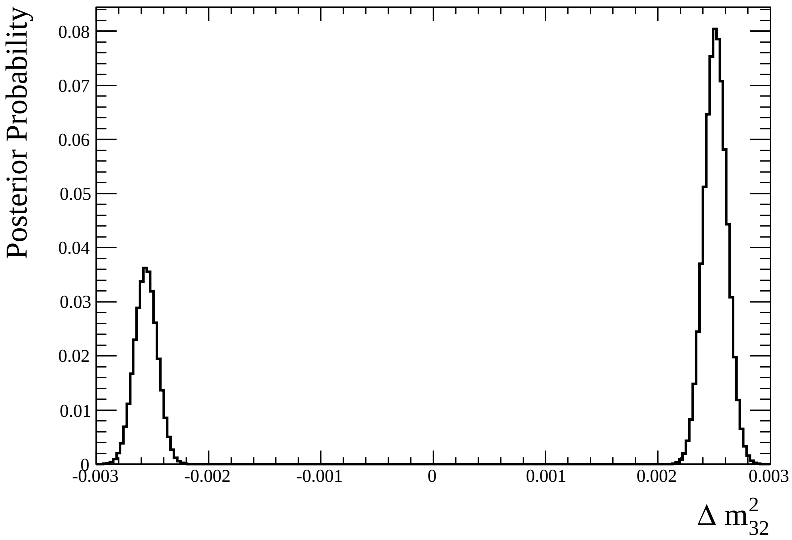

Figure 45: Marginalized Δm^2_{32} posterior. Normal hierarchy is positive values and inverted hierarchy is negative values; 69.1% of the probability lies in the normal hierarchy.

References

[1] C. Bojechko and A. Kaboth. Muon neutrino disappearance simultaneous fit of ND280 and SK with Run 1+2+3 data using Markov Chain Monte Carlo analysis. Technical Report TN-140, T2K, 2013.

[2] C. Bojechko et al. CC multiple pion ν_μ event selections in the ND280 tracker using Run 1+2+3+4 data. Technical Report TN-152, T2K, 2013.

[3] J. Hignight et al. Super-Kamiokande events and data quality studies for T2K Run4. Technical Report TN-148, T2K, 2013.

[4] N. Abgrall et al. Neutrino Flux Prediction for the 2011a Analysis. Technical Report TN-99, T2K, 2011.

[5] P. de Perio et al. Cross section parameters for 2012a oscillation analysis. Technical Report TN-108, T2K, 2012.

[6] P. de Perio et al. Some stuff. Technical Report TN-186, T2K, 2014.

[7] F. James. MINUIT Reference Manual. Technical report, CERN, 2000.

[8] Peter Mills. Efficient statistical classification of satellite measurements. *International Journal of Remote Sensing*, 32 (21):6109–6132, 2011.

[9] M. Hartz, A. Kaboth, and K. Mahn. ND280 Flux and Cross Section Constraint for 2013. Technical Report TN-166, T2K, 2013.

[10] A. Gelman, X.L. Meng, and H. Stern. Posterior predictive assessment of model fitness via realized discrepancies. *Statistica Sinica*, 6:733–759, 1996.

[11] P. Adamson et al. Electron Neutrino and Antineutrino Appearance in the Full MINOS Data Sample. *Phys. Rev. Lett.*, 110:171801, Apr 2013.

A Additional Fake Data Set Plots

A.1 T2K Only

Contour comparison with VALOR analysis.

plots/fds/fds_0_cont_th23dm23-eps-converted-to.pdf

plots/fds/fds_0_cont_th13dcp-eps-converted-to.p

(a) $1\text{R}\nu_\mu$

(b) $1\text{R}\nu_e$

Figure 46: Fake Data Set 0

A.2 T2K with Reactor Constraint

MaCh3 only contours, both hierarchies.

plots/fds/fds_2_cont_th23dm23-eps-converted-to.pdf

(a) 1Rν_μ

plots/fds/fds_2_cont_th13dcp-eps-converted-to.pdf

(b) 1Rν_e

Figure 47: Fake Data Set 2

plots/fds/fds_3_cont_th23dm23-eps-converted-to.pdf

(a) 1Rν_μ

plots/fds/fds_3_cont_th13dcp-eps-converted-to.pdf

(b) 1Rν_e

Figure 48: Fake Data Set 3

plots/fds/fds_4_cont_th23dm23-eps-converted-to-pdf

(a) 1Rν_μ

plots/fds/fds_4_cont_th13dcp-eps-converted-to.pd

(b) 1Rν_e

Figure 49: Fake Data Set 4

plots/fds/fds_5_cont_th23dm23-eps-converted-to-pdf

(a) 1Rν_μ

plots/fds/fds_5_cont_th13dcp-eps-converted-to.pd

(b) 1Rν_e

Figure 50: Fake Data Set 5

plots/fds/fds_1_reactor_contour_th23_dm23-eps-converted-to.pdf

plots/fds/fds_1_reactor_contour_th13_dcp-eps-con

(a) 1Rν_μ

(b) 1Rν_e

Figure 51: Fake Data Set 1

plots/fds/fds_2_reactor_contour_th23_dm23-eps-converted-to.pdf

plots/fds/fds_2_reactor_contour_th13_dcp-eps-con

(a) 1Rν_μ

(b) 1Rν_e

Figure 52: Fake Data Set 2

plots/fds/fds_3_reactor_contour_th23_dm23-eps-converted-to.pdf

(a) 1Rν_μ

plots/fds/fds_3_reactor_contour_th13_dcp-eps-con

(b) 1Rν_e

Figure 53: Fake Data Set 3

plots/fds/fds_4_reactor_contour_th23_dm23-eps-converted-to.pdf

(a) 1Rν_μ

plots/fds/fds_4_reactor_contour_th13_dcp-eps-con

(b) 1Rν_e

Figure 54: Fake Data Set 4

plots/fds/fds_5_reactor_contour_th23_dm23-eps-converted-to.pdf

(a) 1Rν_μ

plots/fds/fds_5_reactor_contour_th13_dcp-eps-con

(b) 1Rν_e

Figure 55: Fake Data Set 5

A.3 Comparison with VALOR

plots/fds/compare_fds_0_reactor_cont_th13dcp-eps-converted-to.pdf

(a) Fake Data Set 0 with Reactor Constraint.

plots/fds/compare_fds_1_reactor_cont_th13dcp-eps

(b) Fake Data Set 1 with Reactor Constraint.

plots/fds/compare_fds_2_reactor_cont_th13dcp-eps-converted-to.pdf

(c) Fake Data Set 2 with Reactor Constraint.

plots/fds/compare_fds_3_reactor_cont_th13dcp-eps

(d) Fake Data Set 3 with Reactor Constraint.

plots/fds/compare_fds_4_reactor_cont_th13dcp-eps-converted-to.pdf

(e) Fake Data Set 4 with Reactor Constraint.

plots/fds/compare_fds_5_reactor_cont_th13dcp-eps

(f) Fake Data Set 5 with Reactor Constraint.